n-Doping of a Low-Electron-Affinity Polymer Used as an Electron-Transport Layer in Organic Light-Emitting Diodes

*Hannah L. Smith, Jordan T. Dull, Elena Longhi, Stephen Barlow, Barry P. Rand, Seth R. Marder, and Antoine Kahn**

Hannah L. Smith, Jordan T. Dull, Prof. Barry Rand, Prof. Antoine Kahn
Department of Electrical Engineering, Princeton University, Princeton, NJ 08544, USA
* E-mail: kahn@princeton.edu

Prof. Barry P. Rand
Andlinger Center for Energy and the Environment, Princeton University, Princeton, NJ 08544, USA

Dr. Elena Longhi, Dr. Stephen Barlow, Prof. Seth R. Marder
School of Chemistry and Biochemistry and Center for Organic Photonics, Georgia Institute of Technology, Atlanta, GA 30332, USA

Keywords: organic semiconductors, n-doping, conductivity, OLEDs

Abstract

n-Doping electron-transport layers (ETLs) increases their conductivity and improves electron injection into organic light-emitting diodes (OLEDs). Because of the low electron affinity and large bandgaps of ETLs used in green and blue OLEDs, n-doping has been notoriously more difficult for these materials. In this work, we demonstrate n-doping of the polymer poly[(9,9-dioctylfluorene-2,7-diyl)-*alt*-(benzo[2,1,3]thiadiazol-4,7-diyl)] (F8BT) via solution processing, using the air-stable n-dopant (pentamethylcyclopentadienyl)(1,3,5-trimethylbenzene)ruthenium dimer $[RuCp^*Mes]_2$. Undoped and doped F8BT films are characterized using ultra-violet and inverse photoelectron spectroscopy. The ionization energy and electron affinity of the undoped F8BT are found to be 5.8 eV and 2.8 eV, respectively. Upon doping F8BT with $[RuCp^*Mes]_2$, the Fermi level shifts to within 0.25 eV of the F8BT lowest unoccupied molecular orbital, which is indicative of n-doping. Conductivity measurements reveal a four order of magnitude increase in the conductivity upon doping and irradiation with ultra-violet light. The $[RuCp^*Mes]_2$-doped F8BT films are incorporated as an

ETL into TPBi:Ir(ppy)$_3$-based green OLEDs, and the luminance is improved by three orders of magnitude when compared to identical devices with an undoped F8BT ETL.

1. Introduction

Electron-transport layers (ETLs) with low electron affinity (EA) and large bandgap are commonly used in green and blue organic light-emitting diodes.[1,2] The typically low EA of the emissive layer requires the ETL to also have a low EA in order to reduce the barrier for electron injection into the emissive layer and, thereby, improve efficiency. The ETL is also generally chosen to have a large energy gap between filled and empty states, ensuring that it also functions as a hole and exciton blocker. Efficient electron injection into a low EA film requires either a low-work-function (WF) electrode or n-doping to create a low effective injection barrier. Over the years, one class of solutions to this problem evolved from the use of low WF metals, such as Ca or Mg-Ag,[3,4] which suffer from a lack of stability and high reactivity, to electrode surface modification via self-assembled monolayers[5] and, more recently, ultra-thin films of polymers containing aliphatic amine groups.[6] The other approach has been to n-dope the ETL in the vicinity of the electrode, thereby lowering the effective injection barrier by moving the interface Fermi level closer to the lowest unoccupied molecular orbital (LUMO) of the ETL, or by creating a narrow depletion region that allows carrier tunneling.[7,8] In addition to enhancing charge injection into the emissive layer, n-doping the ETL also enhances device performance and stability by improving film conductivity, allowing the use of a thicker layer that is more protective against interactions with substrate or subsequent depositions of contacts.

To achieve spontaneous n-doping of a molecular or polymer material through a simple guest-to-host electron-transfer reaction, the dopant must have an ionization energy (IE) comparable to, or lower than, the EA of the host. In the case of the low-EA ETL hosts discussed in this work, n-dopants must have a comparatively low IE, which makes them highly sensitive to oxidation by ambient oxygen or moisture.[9] To address these stability issues, new classes of n-dopants have been developed over the past few years in which chemical reactions are coupled to the electron-transfer process,[10–14] including powerful

reductants based on organometallic dimers that exhibit moderate air-stability in their dimer form.[12,13] One of these dimers, (pentamethylcyclopentadienyl)(1,3,5-trimethylbenzene)ruthenium $[RuCp^*Mes]_2$ (**Figure 1**a), was recently shown to efficiently n-dope several small-molecule ETLs including phenyldi(pyren-2-yl)phosphine oxide ($POPy_2$),[15] in spite of the notably low EA (2.2 eV) of this compound. An EA of 2.2 eV leads to a very large kinetic barrier for reaction with $[RuCp^*Mes]_2$ and, moreover, is even beyond the estimated thermodynamic reducing strength of the dopant; thus, an activation process was necessary to initiate a reaction and achieve n-doping. In this case, this step was in the form of photoactivation of an initial electron transfer from the dimer to the host, immediately followed by dimer cleavage yielding two species, a stable 18-electron cation $RuCp^*Mes^+$ and a highly reducing 19-electron monomer, which in turn donates a second electron to the host. The resulting n-doping of $POPy_2$, as well as that of other ETLs with similarly low EA, was found to be remarkably stable over time.

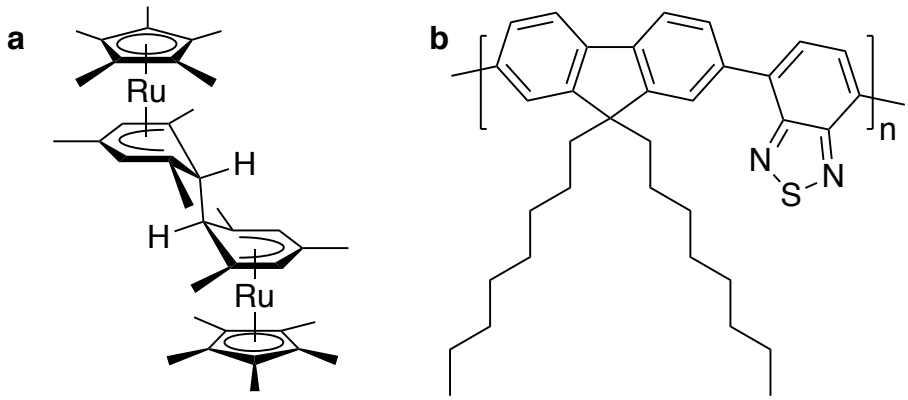

Figure 1. Chemical structures of the (a) dimeric dopant $[RuCp^*Mes]_2$ and (b) host material (F8BT).

In the $POPy_2$ case, both dopant and host were evaporated in an ultra-high vacuum (UHV) system prior to photoactivation of the doping. Although the most efficient photoactivation was achieved by use of photons with energy above the optical gap of $POPy_2$, photons with energy below the onset of absorption of $POPy_2$ also led to doping, but as a result of low oscillator strength charge-transfer (CT) state absorption.[15] The focus of the present

work is to demonstrate the use of solution processing for incorporating $[RuCp^*Mes]_2$ into, and efficiently n-doping, a low EA polymer. n-Doping with the ruthenium-based dimer has been previously demonstrated in solution-processed polymers; however, it has only been used on hosts with significantly larger EA (>3.5-4 eV), including P(BTP-DPP),[16] P(NDI2OD-T2),[17]and FBDPPV,[18] for which the initial electron transfer from the dimer is considerably less endergonic than that to $POPy_2$, leading to facile n-doping. Here, we employ the polymer poly[(9,9-dioctylfluorene-2,7-diyl)-*alt*-(benzo[2,1,3]thiadiazol-4,7-diyl)] (F8BT) (Figure 1b), with a low EA equal to 2.8 eV and which is therefore much more challenging to n-dope. As in the case of $POPy_2$, we observe that photoactivation is required for effective doping; we demonstrate the use of the doped polymer film as an efficient ETL for a green organic light-emitting diode (OLED).

2. Results and Discussion

Direct and inverse photoelectron spectroscopy are used here to measure the energy levels of undoped and doped F8BT films, with particular focus on the shift in the Fermi level between these films. The IE of the polymer measured by ultra-violet photoelectron spectroscopy (UPS) on undoped F8BT is found to be 5.8 eV (**Figure 2**a), in agreement with previously reported values,[19,20] whereas the EA is determined via inverse photoelectron spectroscopy (IPES) and found equal to 2.8 eV. The EA of F8BT has been previously reported to be 3.3 eV for this polymer;[21] however, that value was derived from a combination of IE and the optical gap, neglecting the exciton binding energy, which is typically a few 100 meV in polymer semiconductors. The transport, or single particle, gap of F8BT measured here is IE - EA ~ 3.0 eV. The optical gap of F8BT, measured via direct optical absorption, is found to be 2.4 eV (**Figure 3**), in agreement with previous reports.[22,23]

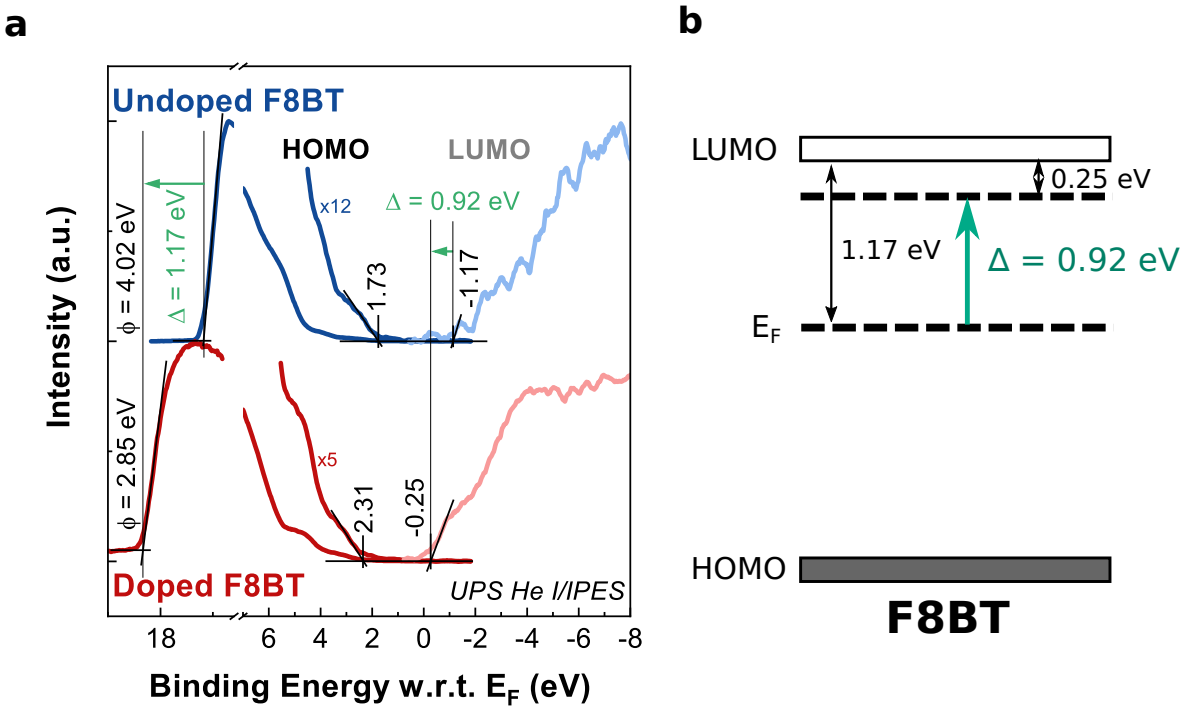

Figure 2. (a) Combined UPS (filled states) and IPES (empty states) spectra for undoped (blue) and 25 wt.% $[RuCp^*Mes]_2$ doped (red) F8BT. The left part of the UPS spectra shows the photoemission cut-offs, from which the vacuum level and WF shifts are determined. EA and IE, measured on the undoped film, are 2.8 eV and 5.8 eV, respectively. The Fermi level shifts upward in the gap by 0.92 eV, from 1.17 eV below to the LUMO to 0.25 eV when the F8BT is doped. Proportionally, the work function decreases by 1.17 eV upon doping, from 4.02 eV to 2.85 eV. (b) Schematic representation of the shift in the Fermi level between the undoped and doped F8BT films.

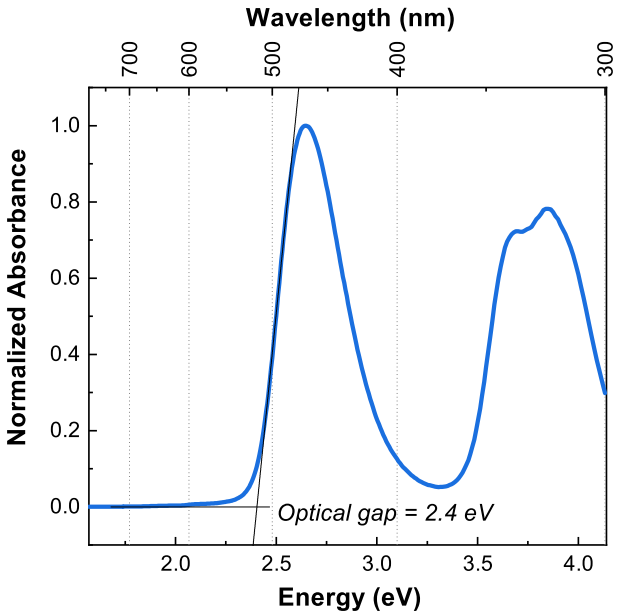

Figure 3. UV-Vis absorption of an undoped F8BT film. The optical gap of the F8BT is determined to be 2.4 eV.

Film preparation and film introduction in the conductivity measurement vacuum chamber were conducted under low light levels in order to reduce as much as possible the unwanted photoactivation of the doping process. However, the films were exposed to some ambient light during the fabrication process. The undoped F8BT has a conductivity of 10^{-10} S cm^{-1}, while the pre-irradiation conductivity of a film cast from a solution containing a 3:1 wt/wt polymer/dopant ratio shows a very small increase to 10^{-9} S cm^{-1} (**Figure 4**a). We cannot rule out some weak photoactivation due to ambient light exposure. Furthermore, deep electron traps in the F8BT gap are presumably kinetically accessible for filling by the dimer, which could initiate the cleavage of a few dopants, and could also increase the conductivity. However, like in the $POPy_2$ case, the complete doping process requires photoactivation. The undoped film exhibited a negligible increase in conductivity upon ultra-violet (UV) irradiation. The doped film photoactivated by a UV light-emitting diode (LED) achieves a conductivity higher than 10^{-7} S cm^{-1} (Figure 4a), a three order of magnitude increase when compared to the undoped film. This increase is found to be stable for over 10 h post-irradiation, in vacuum and in the dark.

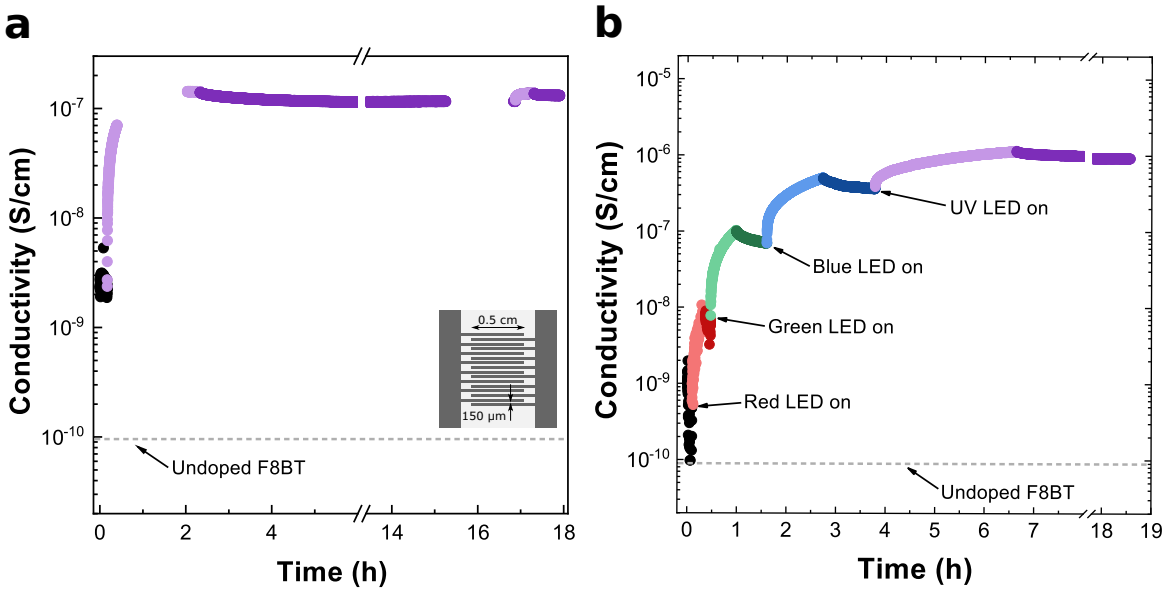

Figure 4. Conductivity vs. time of the doped F8BT film in the dark before illumination (black) and during and after illumination (a) by only a UV LED (375 nm, 3.31 eV) and (b) sequentially by red (660 nm, 1.87 eV), green (530 nm, 2.34 eV), blue (470 nm, 2.64 eV), and

UV LEDs. The lighter colors represent the conductivity while the film is illuminated, and the darker colors are the conductivity while the film is in the dark. Inset: Schematic representation of the interdigitated electrode structure used to measure the conductivity of the F8BT films. The device architecture has 8 long electrodes on each side.

To further examine the effects of irradiation on the dimer cleavage process, a doped film was sequentially irradiated with different photon sources that emit at energies ranging from below to above the F8BT optical bandgap. When $POPy_2$ is doped by the same ruthenium dimer, only UV light with photon energy (3.31 eV) higher than the optical gap of $POPy_2$ (3.1 eV) was able to lead to an increase in conductivity that fully saturated within the time allotted for the experiment (>30 h).[15] With photon energies lower than the bandgap (red, 1.88 eV; green, 2.34 eV; and blue, 2.64 eV), the conductivity increased by several orders of magnitude, but never reached the level of the UV irradiated film. We see a similar relationship between the optical gap of F8BT and the wavelengths of light that efficiently photoactivate the doped film. The blue and UV LED photons have energies higher than the optical gap of F8BT (2.4 eV), and lead to direct absorption excitation of the host. As explained by Lin et al. for the case of $POPy_2$:$[RuCp^*Mes]_2$,[15] this leads to an electron donation from the dimer to the $POPy_2$ excited state, followed by dimer cleavage and second electron donation. In the case of F8BT, both blue and UV photons almost fully saturate the conductivity of the irradiated doped film (Figure 4b). The irradiation time is shorter (~1 h), but the conductivity only increases marginally after about 30 min, so prolonged exposure is unnecessary. For red and green LEDs, the increase in conductivity is much slower due to a less efficient photoactivation process, the energy of the photons being lower than the optical gap of F8BT. By analogy to the $POPy_2$:$[RuCp^*Mes]_2$ case, the likely initial step in this energy range is excitation of a weak dimer-to-host CT absorption;[15] this is immediately followed by dimer cleavage and release of the second electron by the 19-electron monomer.

In the case of $POPy_2$, external quantum efficiency (EQE) measurements revealed a weak absorption attributable to a dimer-to-$POPy_2$ CT state below its optical gap; a single scan

from high photon energy to low photon energy was sufficient to trigger the disappearance of this CT state due to activation of doping. Similarly, we used EQE measurements to probe the evolution of CT state absorption in the F8BT:$[RuCp^*Mes]_2$ system, using the device structure indium tin oxide (ITO)/F8BT/bathocuproine (BCP)/Al (**Figure 5**a), where the F8BT is either undoped or doped. A device with undoped F8BT exhibits two main features centered at 2.6 eV and 3.7 eV (Figure 5b), attributable to absorption by F8BT (Figure 3), and no additional feature below the optical band gap. However, for F8BT doped with $[RuCp^*Mes]_2$, initial EQE scans reveal a broad absorption feature below the F8BT optical gap that we attribute to CT; consistent with this assignment, this feature is seen at a somewhat lower energy than the CT band of $POPy_2$:$[RuCp^*Mes]_2$, as expected given the slightly larger EA of F8BT. The doped devices were first scanned from low photon energy to high photon energy (scan 1), and then from high photon energy to low photon energy (scan 2). For this material system, the light generated by the EQE setup was not sufficiently strong to lead to doping. In order to expedite the doping process, the EQE devices with doped F8BT were placed under the light of a solar simulator (AM1.5) for 1 h to more efficiently activate the doping. After the prolonged light exposure, the strength of the CT feature decreased significantly (scan 3), as well as that of the main absorption feature centered at 2.6 eV. The reduction in the CT signal, like in the $POPy_2$ case,[15] is consistent with a reduction in the number of neutral dimers via cleavage upon photoactivation of the doping process. On the other hand, the reduction and fluctuations in the polymer part of the EQE signal (2.6 and 3.7 eV features) are more difficult to explain, but are likely linked to changes in the photogeneration, transport, and/or recombination of free electrons and holes in the EQE device upon introduction of the dopants. After some recovery time in the dark, (1 h, scan 4, and 5 h, scan 5), the 2.6 eV peak recovers, but the CT state feature remains diminished. This experiment suggests, therefore, that the doping mechanism for $[RuCp^*Mes]_2$ in F8BT is similar to that in $POPy_2$. However, one noticeable difference is that the CT state feature does not fully disappear in the doped F8BT, even after prolonged

light exposure. This highlights a less efficient doping process in the polymer film, where, despite photocurrent generation (i.e. finite EQE), some of these CT photocurrent generation events do not lead to doping. This is consistent with the more moderate increase in conductivity seen in the doped F8BT film (10^{-6} S cm^{-1}) when compared to the doped $POPy_2$ film (10^{-4} S cm^{-1}).

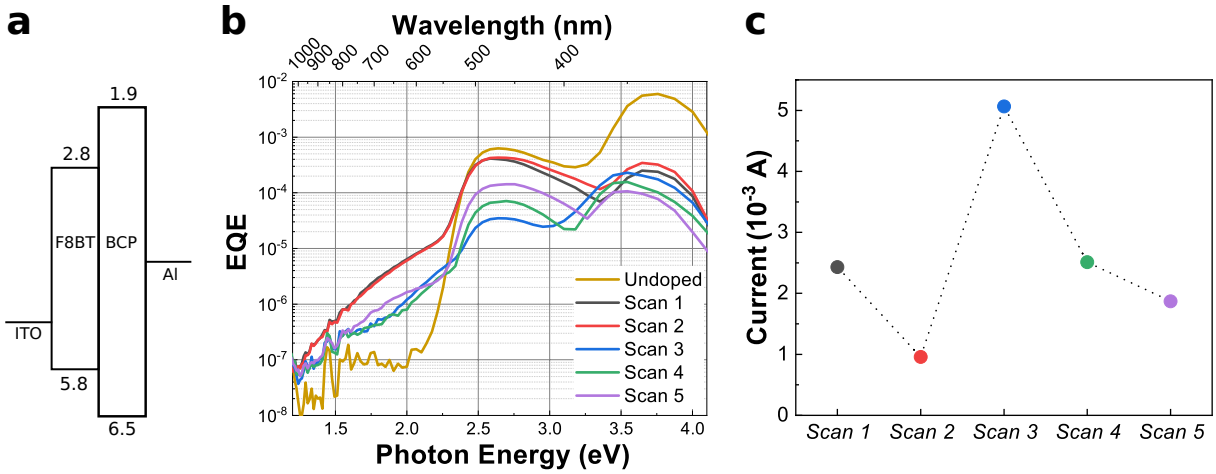

Figure 5. (a) Energy diagram for the device used for external quantum efficiency (EQE) measurements. The IE and EA for BCP are from ref. [24] (b) EQE scans of the undoped and doped F8BT devices. There is one scan of an undoped device (yellow) for reference, and several sequential scans of a doped device. For scan 1, the photon energy was swept from low photon energy to high photon energy, and the reverse was done for scan 2. Before scan 3, the doped device was exposed to the light of a solar simulator for 1 h. Scan 4 was measured after the device recovered for 1 h, and scan 5 was measured 4 h post light exposure. (c) A measurement of the current at -2 V for the same doped F8BT EQE device was done before each EQE measurement.

To further probe the evolution of the properties of the doped layer throughout these EQE measurements, we measured the current versus voltage for the same device measured with the EQE setup, before each EQE measurement, as shown in Figure 5b. The maximum current in the device decreases after the first EQE scan (Figure 5c), but significantly increases after exposure to the solar simulator for 1 h (scan 3), consistent with the higher conductivity of the F8BT layer following dopant activation. For the two subsequent scans after recovery (scans 4 and 5), the current decreases. We hypothesize that the drop in current between scan 1 and scan 2 is due to the effect of removing the low-vacuum box containing the sample from the glovebox for the EQE measurement; ambient air slowly leaks in through the valve during

the experiment and may introduce oxygen-related electron traps in the polymer film. After illumination in the solar simulator for 1 h, the current increases, indicating photo-activated n-doping. After the film recovers in the dark for 1 h (scan 4) and 5 h (scan 5), the current decreases again, likely due to de-doping from a small concentration of oxygen in the glove box. Note that the conductivity of the F8BT:$[RuCp^*Mes]_2$ system is highly stable in UHV, at a base pressure of 10^{-10} Torr (Figure 4).

To demonstrate one of the applications of n-doped F8BT, OLEDs were fabricated using the polymer as the electron injection and transport layer. The device structure used for these OLEDs was ITO/poly(3,4-ethylenedioxythiophene) polystyrene sulfonate (PEDOT:PSS)/F8BT/1,3,5-tris(1-phenyl-1*H*-benzo[*d*]imidazol-2-yl)benzene (TPBi)/TPBi: tris[2-phenylpyridinato-C^2,N]iridium(III) ($Ir(ppy)_3$)/tris(4-carbazoyl-9-ylphenyl)amine (TCTA)/4,4′-(cyclohexan-1,1-diyl)bis[*N*,*N*-di(4-tolyl)aniline (TAPC)/MoO_3/Al, where TPBi:$Ir(ppy)_3$ serves as the green-emitting layer and TAPC and TCTA are hole-injection and electron-blocking layers, respectively (**Figure 6**a). The high-work-function (~5.0 eV) PEDOT:PSS, typically used for hole injection, was used instead on the electron-injection side to demonstrate the ability to reduce the electron-injection barrier via n-doping of the ETL, thus making the work function of the contact material nearly irrelevant. OLEDs were fabricated with both undoped and doped F8BT as the ETL. To achieve high conductivity (Figure 4), the doped F8BT was irradiated with a UV lamp for 10 min after the film was annealed, but before the emissive and subsequent layers were deposited.

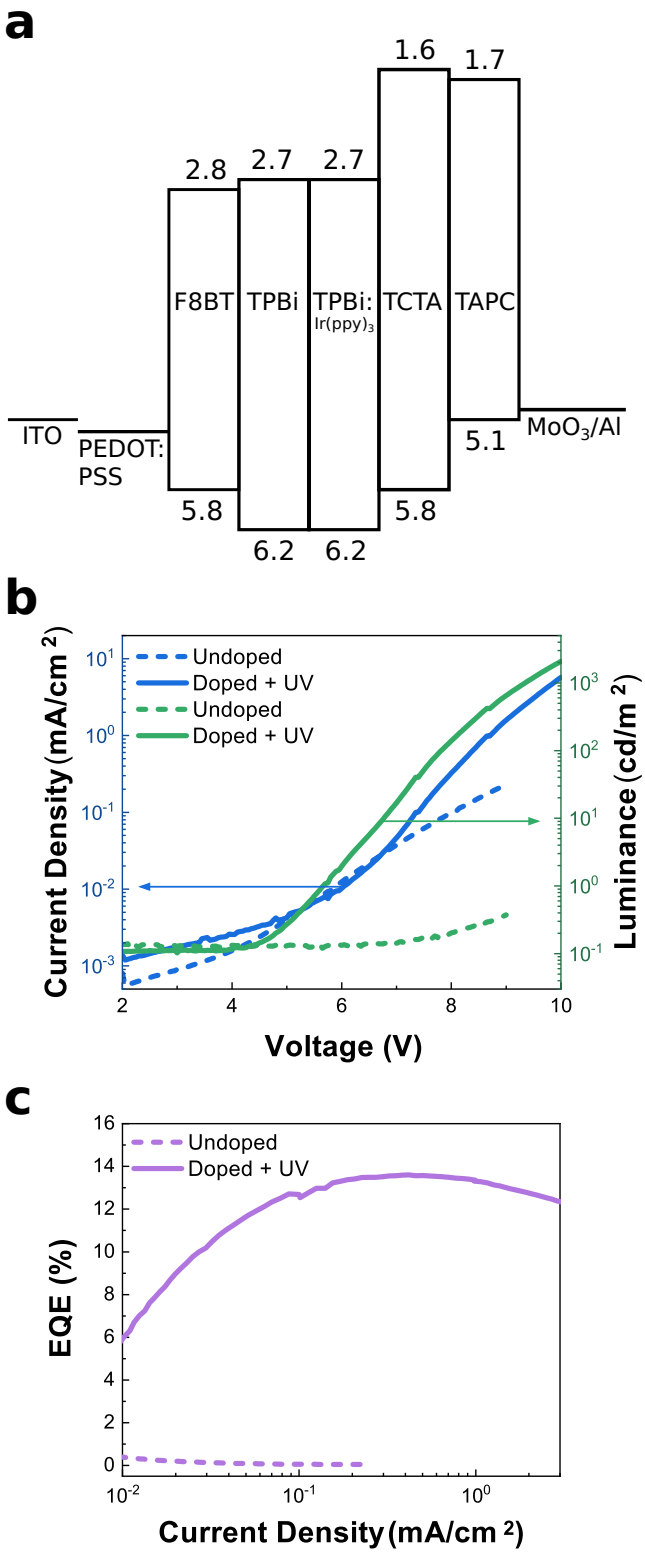

Figure 6. (a) Energy diagram of a green emitting OLED using TPBi:Ir(ppy)$_3$ as the emissive layer. The IE and EA for TPBi, TCTA, and TAPC are from references [24,25]. Undoped and doped F8BT was used as an electron transport layer. (b) Current density and luminance vs. voltage for the undoped F8BT and the F8BT that was doped with [RuCp*Mes]$_2$ and UV activated for 10 min. (c) EQE vs. current density for the undoped and doped F8BT.

Because of the large electron-injection barrier, OLEDs with undoped F8BT displayed a low current density, predominantly due to holes, since electrons are effectively blocked (Figure 6b). This results in negligible luminance from the device. In the OLEDs with the doped F8BT ETL, the current density increases and the luminance increases by over three orders of magnitude to above 10^3 cd m^{-2}. Several scans of the device are provided in **Figure S1**. The EQE of the devices with doped F8BT reaches nearly 14%, (Figure 6c), which is in line with the results reported by Lin et al. for a similar OLED structure with n-doped $POPy_2$ as the ETL doped with $[RuCp^*Mes]_2$.[15]

3. Summary

This work demonstrates that solution processing, followed by photoactivation, can be used to n-dope the low EA (2.8 eV) polymer F8BT with the organometallic ruthenium-based $[RuCp^*Mes]_2$ dimer. UV irradiation of the F8BT:$[RuCp^*Mes]_2$ film initiates electron transfer from the dimer to the polymer, followed by dimer cleavage, and release of a second electron. Both Fermi-level movement to 0.25 eV below the F8BT LUMO and a rise in conductivity by four orders of magnitude to 10^{-6} S cm^{-1} confirm n-doping. As in the case of $POPy_2$:$[RuCp^*Mes]_2$, doping remains stable with time in vacuum and in the dark, in spite of the fact that F8BT is close to the limit of the thermodynamic reducing strength of the $[RuCp^*Mes]_2$ dimer. The TPBi:$Ir(ppy)_3$-based green OLEDs fabricated with an intentionally high injection barrier between the cathode and F8BT show considerably improved device performance, including a three order of magnitude increase in luminance, when the F8BT injection layer is doped. Devices with the doped ETL have an EQE of nearly 14% (nearly 0% for the undoped ETL). The efficacy of these air-stable, highly reducing n-type dopants is, therefore, clearly demonstrated in solution-processed OLED ETLs.

4. Experimental Section

Substrate and Solvent Preparation: ITO-on-glass substrates (quartz for absorption) were sonicated in acetone, isopropanol, and then exposed to UV-ozone, each for 10 min, and transferred to a nitrogen glovebox. F8BT (purchased from Sigma Aldrich) was dissolved in chlorobenzene and stirred at 80 °C for 1 h. The concentration of the F8BT solution was 6.67 mg mL^{-1} for photoelectron spectroscopy, 15 mg mL^{-1} for absorption and conductivity measurements, and 10 mg mL^{-1} for OLEDs. $[RuCp^*Mes]_2$ (synthesis described elsewhere[18]) was dissolved in toluene and stirred at 80 °C for 1 h. Doped F8BT:$[RuCp^*Mes]_2$ films with desired dopant concentration were spin-coated from solutions made by mixing appropriate amounts of the F8BT and dopant solutions. The mixed solutions were then stirred at 80 °C for 30 min, and spin-coated onto the substrates at 2000 rpm for 45 s. The films were then immediately annealed at 100 °C for 10 min.

UPS and IPES: Samples were transferred without exposure to air into the UHV analysis chamber (base pressure of 5 × 10^{-10} Torr) for ultra-violet and inverse photoelectron spectroscopy (UPS and IPES). For UPS, the He I (21.22 eV) photon line generated by a discharge lamp was used to measure the occupied states of the material. IPES, done in the isochromat mode, was used to measure the unoccupied states in the material (setup described elsewhere).[26] The energy resolution for UPS and IPES is 150 meV and 450 meV, respectively.

UV-Vis Absorption Measurements: An Agilent Technologies Cary 5000 UV-vis-NIR spectrometer was used for absorption. Films were prepared on quartz substrates cleaned by the process described in the substrate preparation section.

Conductivity Measurements: An interdigitated electrode structure was patterned onto quartz substrates by evaporating 100 nm of aluminum through a shadow mask in a thermal

evaporator (Angstrom Engineering). The interdigitated electrode pattern consisted of 8 thin electrodes connected to a larger contact on either side. The spacing between the electrodes was 150 µm (inset of Figure 4a). The quartz substrates were cleaned according to the procedure described in the sample preparation section. The undoped and doped F8BT films were spin-coated in a N_2 glovebox and then transferred to a UHV system for measurement, without exposure to air. The light exposure of the doped film was minimized prior to photoactivation, but not completely eliminated. For photoactivation, samples were illuminated with LEDs from Thorlabs: red [M660L4], green [M530L3], blue [M470L3], and UV [M375L3].

External Quantum Efficiency Measurements: Glass substrates patterned with two strips of ITO were sonicated in acetone and isopropanol for 10 min each, and then exposed to O_2 plasma for 5 min. Undoped and 15 wt.% doped F8BT (which corresponds to a molar ratio of 0.066 or 1:15 RuCp*Mes monomer to F8BT monomers) were spin-coated onto the substrates at 2000 rpm for 30 s and then the films were annealed at 100 °C for 10 min. The substrates were transferred from the solvent glovebox to a dry glovebox without air exposure, and a thermal evaporator was used to deposit 10 nm of BCP [bathocuproine] and 100 nm of aluminum through a shadow mask. For the EQE measurements, the substrates were transferred to a vacuum-sealed box and removed from the glovebox. The EQE measurements were taken using a Newport TLS-300X tunable light source system. Measurements were performed under short-circuit conditions using a Stanford Research Systems SR830 lock-in amplifier and SR570 current preamplifier to detect the photocurrent produced by the device from the incident chopped (150 Hz) light. Calibrated Si photodetectors (Newport) served as a reference cell. A solar simulator (ABET Technologies) calibrated for 1 sun AM1.5G illumination was used to expose the devices to light for a length of time as noted in the text. Current-voltage characteristics were measured using a Keithley 2602B source meter.

Organic Light-Emitting Diode Measurements: Patterned ITO substrates were sonicated in acetone and isopropanol for 10 min each, and then treated with O_2 plasma for 5 min. PEDOT:PSS was spin-coated onto the substrates at 2000 rpm for 30 s and then the films were annealed for 10 min at 150 °C. The substrates were then immediately transferred to a solvent N_2 glovebox where both undoped and doped (20 wt.%) F8BT solutions (10 mg mL^{-1}) were spin-coated at 2000 rpm for 45 s. The films were annealed at 100 °C for 10 min and transferred to a dry N_2 glovebox without exposure to air. The doped F8BT was exposed to a UV lamp for 10 min to photoactivate the doping process. The substrates were transferred into a thermal evaporator to deposit the remaining layers of the OLED: 10 nm TPBi [1,3,5-tris(1-phenyl-1*H*-benzo[*d*]imidazol-2-yl)benzene], 10 nm TPBi with 4% $Ir(ppy)_3$ [tris[2-phenylpyridinato-C^2,N]iridium(III)], 15 nm TCTA [tris(4-carbazoyl-9-ylphenyl)amine], 50 nm TAPC [4,4′-(cyclohexan-1,1-diyl)bis[*N*,*N*-di(4-tolyl)aniline], 5 nm MoO_3, and 100 nm aluminum through a shadow mask.

Acknowledgements

This work was supported in part by a grant of the National Science Foundation (DMR-1807797) (HLS, EL, SB, BPR, SRM, AK), by a National Science Foundation Graduate Research Fellowship (DGE-1656466) (HLS), and by a grant from the Department of Energy Office of Basic Energy Sciences, Division of Materials Sciences and Engineering under Award #DE-SC0012458 (JTD, BPR, AK). The authors acknowledge the use of the Cary 5000 UV-vis-NIR spectrometer in the Princeton's Imaging and Analysis Center, which is partially supported by the Princeton Center for Complex Materials, a National Science Foundation (NSF)-MRSEC program (DMR-1420541).

Received: ((will be filled in by the editorial staff))
Revised: ((will be filled in by the editorial staff))
Published online: ((will be filled in by the editorial staff))

References

[1] I. S. Park, S. Y. Lee, C. Adachi, T. Yasuda, *Adv. Funct. Mater.* **2016**, *26*, 1813.

[2] T. Miwa, S. Kubo, K. Shizu, T. Komino, C. Adachi, H. Kaji, *Sci. Rep.* **2017**, *7*, 1.

[3] S. Schubert, J. Meiss, L. Müller-Meskamp, K. Leo, *Adv. Energy Mater.* **2013**, *3*, 438.

[4] S. T. Lee, Z. Q. Gao, L. S. Hung, *Appl. Phys. Lett.* **1999**, *75*, 1404.

[5] B. De Boer, A. Hadipour, M. M. Mandoc, P. W. M. Blom, *Mater. Res. Soc. Symp. Proc.* **2005**, *871*, 189.

[6] Y. Zhou, C. Fuentes-Hernandez, J. Shim, J. Meyer, A. J. Giordano, H. Li, P. Winget, T. Papadopoulos, H. Cheun, J. Kim, M. Fenoll, A. Dindar, W. Haske, E. Najafabadi, T. M. Khan, H. Sojoudi, S. Barlow, S. Graham, J.-L. Brédas, S. R. Marder, A. Kahn, B. Kippelen, *Science (80-.).* **2012**, *336*, 327.

[7] W. Gao, A. Kahn, *Appl. Phys. Lett.* **2001**, *79*, 4040.

[8] W. Gao, A. Kahn, *J. Appl. Phys.* **2003**, *94*, 359.

[9] I. E. Jacobs, A. J. Moulé, *Adv. Mater.* **2017**, *29*, 1.

[10] P. Wei, J. H. Oh, G. Dong, Z. Bao, *J. Am. Chem. Soc.* **2010**, *132*, 8852.

[11] B. D. Naab, S. Guo, S. Olthof, E. G. B. Evans, P. Wei, G. L. Millhauser, A. Kahn, S. Barlow, S. R. Marder, Z. Bao, *J. Am. Chem. Soc.* **2013**, *135*, 15018.

[12] S. Guo, S. K. Mohapatra, A. Romanov, T. V. Timofeeva, K. I. Hardcastle, K. Yesudas, C. Risko, J. L. Brédas, S. R. Marder, S. Barlow, *Chem. Eur. J.* **2012**, *18*, 14760.

[13] S. Guo, S. B. Kim, S. K. Mohapatra, Y. Qi, T. Sajoto, A. Kahn, S. R. Marder, S. Barlow, *Adv. Mater.* **2012**, *24*, 699.

[14] P. Wei, T. Menke, B. D. Naab, K. Leo, M. Riede, Z. Bao, *J. Am. Chem. Soc.* **2012**, *134*, 3999.

[15] X. Lin, B. Wegner, K. M. Lee, M. A. Fusella, F. Zhang, K. Moudgil, B. P. Rand, S. Barlow, S. R. Marder, N. Koch, A. Kahn, *Nat. Mater.* **2017**, *16*, 1209.

[16] E. E. Perry, C. Y. Chiu, K. Moudgil, R. A. Schlitz, C. J. Takacs, K. A. O'Hara, J. G.

Labram, A. M. Glaudell, J. B. Sherman, S. Barlow, C. J. Hawker, S. R. Marder, M. L. Chabinyc, *Chem. Mater.* **2017**, *29*, 9742.

[17] Y. Zhang, H. Phan, H. Zhou, X. Zhang, J. Zhou, K. Moudgil, S. Barlow, S. R. Marder, A. Facchetti, T. Q. Nguyen, *Adv. Electron. Mater.* **2017**, *3*.

[18] H. I. Un, S. A. Gregory, S. K. Mohapatra, M. Xiong, E. Longhi, Y. Lu, S. Rigin, S. Jhulki, C. Y. Yang, T. V. Timofeeva, J. Y. Wang, S. K. Yee, S. Barlow, S. R. Marder, J. Pei, *Adv. Energy Mater.* **2019**, *9*, 1.

[19] M. C. Gwinner, Y. Vaynzof, K. K. Banger, P. K. H. Ho, R. H. Friend, H. Sirringhaus, *Adv. Funct. Mater.* **2010**, *20*, 3457.

[20] A. L. Shu, A. Dai, H. Wang, Y. L. Loo, A. Kahn, *Org. Electron.* **2013**, *14*, 149.

[21] J. Zaumseil, C. L. Donley, J. S. Kim, R. H. Friend, H. Sirringhaus, *Adv. Mater.* **2006**, *18*, 2708.

[22] H. Ohkita, S. Cook, T. A. Ford, N. C. Greenham, J. R. Durrant, *J. Photochem. Photobiol. A Chem.* **2006**, *182*, 225.

[23] A. C. Arias, N. Corcoran, M. Banach, R. H. Friend, J. D. MacKenzie, W. T. S. Huck, *Appl. Phys. Lett.* **2002**, *80*, 1695.

[24] H. Yoshida, K. Yoshizaki, *Org. Electron.* **2015**, *20*, 24.

[25] J. S. Swensen, E. Polikarpov, A. Von Ruden, L. Wang, L. S. Sapochak, A. B. Padmaperuma, *Adv. Funct. Mater.* **2011**, *21*, 3250.

[26] C. I. Wu, Y. Hirose, H. Sirringhaus, A. Kahn, *Chem. Phys. Lett.* **1997**, *272*, 43.

The table of contents entry should be 50–60 words long and should be written in the present tense and impersonal style (i.e., avoid we). The text should be different from the abstract text.

Keyword: n-doping

Hannah L. Smith, Jordan T. Dull, Elena Longhi, Stephen Barlow, Barry P. Rand Seth R. Marder, and Antoine Kahn*

n-Doping of a Low-Electron-Affinity Polymer Used as an Electron-Transport Layer in Organic Light-Emitting Diodes

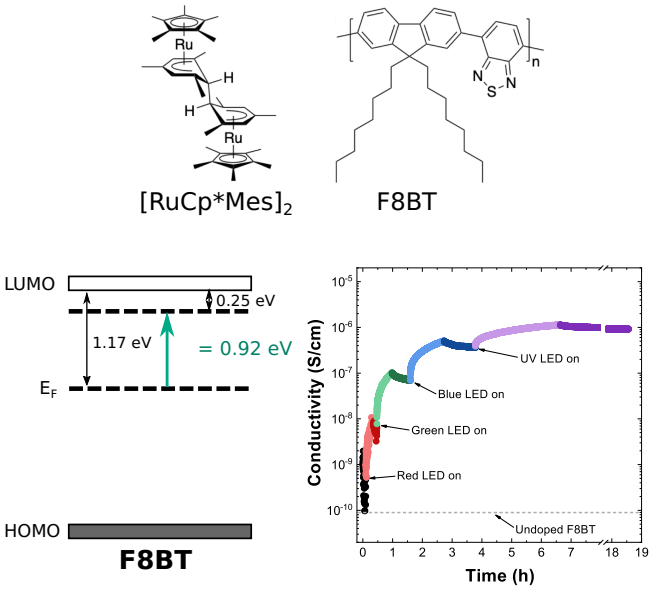

TOC Text:

*The n-dopant (pentamethylcyclopentadienyl)(1,3,5-trimethylbenzene)ruthenium [RuCp*Mes]$_2$ is incorporated into the polymer poly(9,9-dioctylfluorene-alt-benzothiadiazole) (F8BT) via solution processing. Successful n-doping is verified using photoelectron spectroscopy and conductivity measurements. When the doped F8BT film is used as an electron-transport layer in green organic light-emitting diodes, the luminance and external quantum efficiency are improved, relative to the same devices with an undoped F8BT film.*

Supporting Information

n-Doping of a Low-Electron-Affinity Polymer Used as an Electron-Transport Layer in Organic Light-Emitting Diodes

Hannah L. Smith, Jordan T. Dull, Elena Longhi, Stephen Barlow, Barry P. Rand, Seth R. Marder, and Antoine Kahn

The full operational lifetime of the OLEDs was not measured but the OLEDs with the doped F8BT ETL were measured from 2-10 V ten consecutive times (**Figure S1**). The lifetime of OLEDs with the undoped F8BT ETL was not measured due to the initial very poor performance shown in Figure 6.

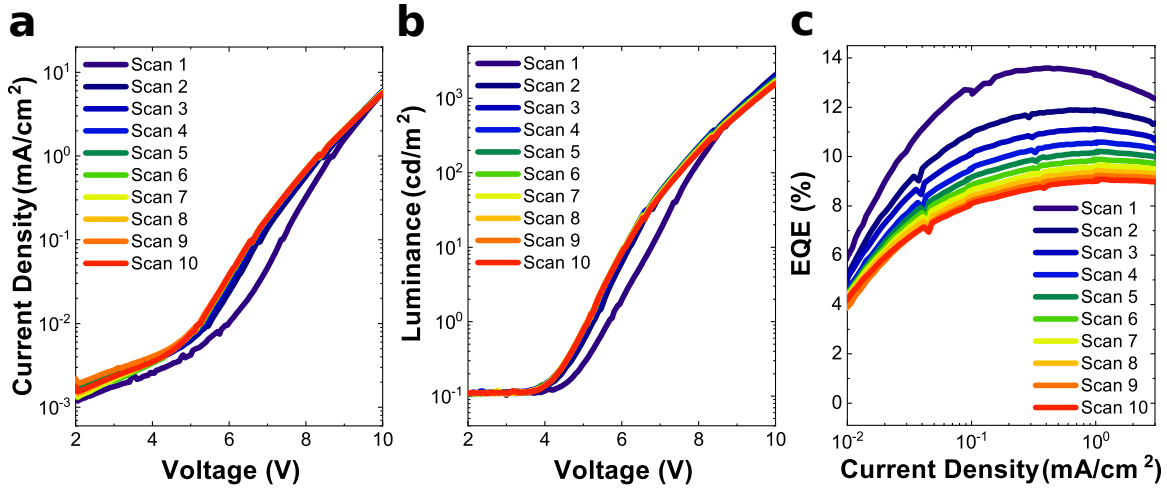

Figure S1. Device characteristics for the TPBi:Ir(ppy)3 based OLEDs with a doped F8BT ETL that was irradiated by UV for 10 min. The first scan of this device is also shown in Figure 6 of the main text. (a) Current density vs. voltage, (b) luminance vs. voltage, and (c) EQE vs. current density.

The current density and luminance of the doped ETL OLED remain fairly stable after an initial shift to a lower turn on voltage (Figure S1a and S1b). The EQE (Figure S1c) shows a steady decrease over time, but it appears to decrease less significantly with each consecutive scan. Each scan takes about 2 minutes, so the total measurement time for this device was approximately 20 minutes.

The overall point of fabricating OLEDs in this work was to demonstrate the use of our solution-processed doped F8BT ETL in an application relevant to the device community. While there is certainly room for enhancing the OLED performance, the focus of this work was on studying $[RuCp^*Mes]_2$ in F8BT.